Supporting Information

Fan et al. 10.1073/pnas.1221817110

SI Materials and Methods

Site-Directed Mutagenesis, Expression, and Purification of the N110C Mutant. The mutation N110C was introduced to pET11b(+)-migration inhibitory factor (MIF) plasmid by site-specific mutagenesis using the QuikChange Site-Directed Mutagenesis Kit (Stratagene). The pET-11b(+)-N110C-MIF plasmid was transformed into the *Escherichia coli* BL21(DE3). Expression and purification of the proteins were performed as previously described for the WT MIF (1). The resulting locked trimer (LT) MIF sample was >95% pure. The ^{15}N-MIF was prepared as previously described (2).

Enzymatic Activity, Receptor Binding, and ERK Signaling Studies. Enzymatic studies used *p*-hydroxyphenylpyruvate as the substrate and the keto/enol tautomerase activity was monitored as previously described (2). To measure the binding of the N110C LT mutant to CD74, a capture assay was used (3). For signaling studies, the effect of MIF and/or N110C on ERK-1/2 activation was examined by Western blotting with Abs specific for phosphorylated (activated) ERK-1/2 (sc-7383; Santa Cruz Biotechnology) in human fibroblast-like synoviocytes (408RA-05a; Cell Applications Inc.). The membrane was then stripped and reprobed with ERK-1/2 Ab specific for total ERK-1/2 to normalize for differences in protein loading (sc-94; Santa Cruz Biotechnology). Quantitation of each blot was measured using ImageJ software and is the ratio of pERK-1/2 to total ERK normalized to 100 for no MIF.

Murine in Vivo Recruitment of Neutrophils to the Lung. C57BL/6J mice (8–12 wk old) had recombinant murine MIF (1 μg in 50 μL normal saline) or LT (1 μg and 5 μg in 50 μL normal saline) directly administered via the intratracheal route (4). After 6 h, three lavages of 0.7 mL were collected. The bronchoalveolar lavage (BAL) fluid was pooled and immediately processed for differential cell counts. The differential cell counts were performed on cytocentrifuge preparations stained with HEMA 3 stain set (Fisher Scientific). A minimum of 200 cells were counted for the differential cell count (5). Total protein was measured using the DC Protein Assay (Bio-Rad) per the manufacturer's recommendations, as previously described (6).

For all mice experiments, the use and care of animals was approved by the Institutional Animal Care and Use Committee at Yale University.

CD Spectroscopy. CD data were recorded using Applied Photophysics spectrometers with thermoelectric temperature control. Far-UV CD and thermostability studies were recorded from LT MIF and WT MIF with 50 μg/mL protein concentration in 20 mM Tris·HCl, 20 mM NaCl (pH 7.5), with a temperature ramp of 1 °C/min. The ellipticity was monitored at 212 nm. Following the buffer baseline subtraction, the CD data were normalized to protein concentration and expressed as a mean residue ellipticity.

Size Exclusion and Light Scattering. The light-scattering (LS) data were collected using a Superdex 75 HR 10/30 size-exclusion chromatography (SEC) column (GE Healthcare) connected to the autosampler-equipped HPLC Agilent 1200. The elution from SEC was monitored by a photodiode array UV-visible detector (Agilent Technologies), differential refractometer (Optilab rEx; Wyatt Corp.), and static and dynamic multiangle laser LS detector (HELEOS II with quasi-elastic LS capability; Wyatt Corp.). Two software packages were used for data collection and analysis: ChemStation (Agilent Technologies) controlled the HPLC operation and data collection from the multiwavelength UV-visible detector, and ASTRA (Wyatt Corp.) collected data from the refractive index detector and the LS detectors, and recorded the UV trace at 280 nm sent from the photodiode array detector. The weight average molecular masses were determined across the entire elution profile in the intervals of 1 s from static LS measurement using ASTRA as previously described (7). Hydrodynamic radii were measured from an "on-line" dynamic LS measurement every 2 s. The dynamic LS signal was analyzed by the method of cumulants (8).

For comparison of elution peaks from WT MIF, N110C, and a mixture of the two proteins, a Sepharose 75 16/60 was used.

Crystallization and Data Collection. Purified protein was concentrated to 22 mg/mL for crystallization. Initial screening for crystallization conditions was performed using Crystal I and II (Hampton Research) screening conditions and a mosquito crystallization robot (TTP LabTech) to dispense 100 nL of protein solution mixed in a 1:1 ratio with the reservoir solution. Drops were equilibrated over 100 μL of reservoir solution using the hanging-drop vapor diffusion method at 293 K. The initial crystallization condition was further optimized using a 24-well crystallization plate with the hanging-drop vapor diffusion method. Each well contained 500 μL of reservoir solution, and the drop contained equal volumes of protein and reservoir solution. Diffraction-quality crystals were obtained under a condition of 0.2 M LiSO4, 0.1 M Tris (pH 8.5), and 33% polyethylene glycol 3350 at 293 K and grew to dimensions of 300 × 100 × 50 μm within 3 d. Before X-ray diffraction experiments, crystals were soaked in reservoir solution containing an additional 15% DMSO and flash-cooled in liquid nitrogen. X-ray diffraction data sets for the crystals were collected at 95 K on beamline X25 at the Brookhaven National Synchrotron Light Source (BNLS) using a wavelength of 1.100 Å and a charge-coupled device detector (Quantum 270; Area Detector Systems Corporation). The diffraction data were integrated, scaled, and averaged using the HKL-2000 program suite (9).

Structure Determination and Refinement. Initial phase determination was performed by molecular replacement using the program Phaser (10) in the CCP4 program suite. The atomic coordinates of WT MIF (1MIF) with some modifications was used as a search model. Model reconstruction was conducted manually with Coot (11). Crystallographic refinement was performed using the program Phenix (12). The loop positions were further refined using composite omit maps using averaging over the threefold noncrystallography symmetry, calculated using Phenix, and displayed in Coot. Some regions have elevated B-factors, which are mostly likely due to the loss of a number of loop-stabilizing interactions. Water molecules and solvent molecules were added to the structure using Phenix on the basis of F_o–F_c map at or above 3.0σ level. After completion of refinement, the final R_{work} and R_{free} were calculated, respectively. Detailed statistics of data collection and refinement with the final model described below are provided in Table S1. The model was checked for errors using RPOCHECK. As a final check on the model, the stereochemical quality was assessed using the program MolProbity (13). Some residues were omitted from the deposited structure owing to extremely weak electron density. The final model consisting of residues for each monomer is listed in Table S2. All figures were prepared using PyMOL (DeLano Scientific). Atomic coordinates and structural factors have been deposited in the Protein Data Bank (PDB ID code 4GUM).

1. Sun HW, Bernhagen J, Bucala R, Lolis E (1996) Crystal structure at 2.6-A resolution of human macrophage migration inhibitory factor. *Proc Natl Acad Sci USA* 93(11):5191–5196.
2. Cho Y, et al. (2010) Allosteric inhibition of macrophage migration inhibitory factor revealed by ibudilast. *Proc Natl Acad Sci USA* 107(25):11313–11318.
3. Fingerle-Rowson G, et al. (2009) A tautomerase-null MIF gene knock-in in mouse reveals that protein interactions and not enzymatic activity mediate MIF-dependent growth regulation. *Mol Cell Biol* 29:1922–1932.
4. Takahashi K, et al. (2009) Macrophage CD74 contributes to MIF-induced pulmonary inflammation. *Respir Res* 10:33.
5. Rajasekaran D, et al. (2012) A model of GAG/MIP-2/CXCR2 interfaces and its functional effects. *Biochemistry* 51(28):5642–5654.
6. Bhandari V, et al. (2012) Increased hyperoxia-induced lung injury in nitric oxide synthase 2 null mice is mediated via angiopoietin 2. *Am J Respir Cell Mol Biol* 46(5):668–676.
7. Folta-Stogniew E, Williams KR (1999) Determination of molecular masses of proteins in solution: Implementation of an HPLC size exclusion chromatography and laser light scattering service in a core laboratory. *J Biomol Tech* 10(2):51–63.
8. Koppel DE (1972) Analysis of macromolecular polydispersity in intensity correlation spectroscopy: The method of cumulants. *J Chem Phys* 47:4814–4820.
9. Otwinowski Z, Minor W (1997) Processing of X-ray diffraction data collected in oscillation mode. *Methods In Enzymology* 276:307–325.
10. Vagin A, Teplyakov A (1997) MOLREP: An automated program for molecular replacement. *J Appl Crystallogr* 30(6):1022–1025.
11. Emsley P, Cowtan K (2004) Coot: Model-building tools for molecular graphics. *Acta Crystallogr D Biol Crystallogr* 60(Pt 12 Pt 1):2126–2132.
12. Terwilliger TC, et al. (2008) Iterative model building, structure refinement and density modification with the PHENIX AutoBuild wizard. *Acta crystallographica. Section D, Biological crystallography* 64(Pt 1):61–69.
13. Lovell SC, et al. (2003) Structure validation by Calpha geometry: Phi,psi and Cbeta deviation. *Proteins* 50(3):437–450.

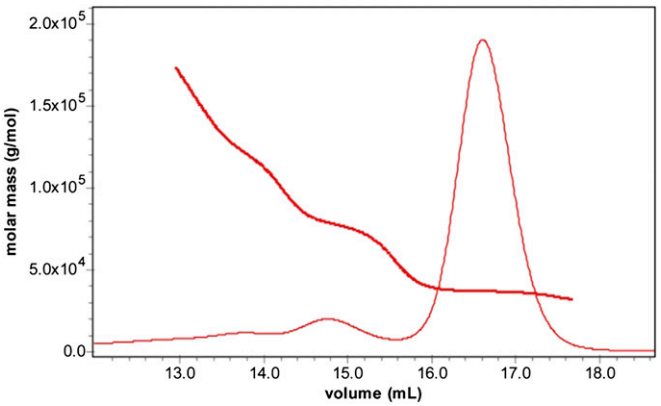

Fig. S1. SEC with LS of the N110C mutant. The peaks of the eluted volume from the SEC 75 (10/30) column for the N110C mutant are overlaid with static LS data from which the molar mass is calculated, and indicate there is one prominent trimer and lower amounts of two and three N110C trimer mutants. The molar mass was calculated as described in *SI Materials and Methods*.

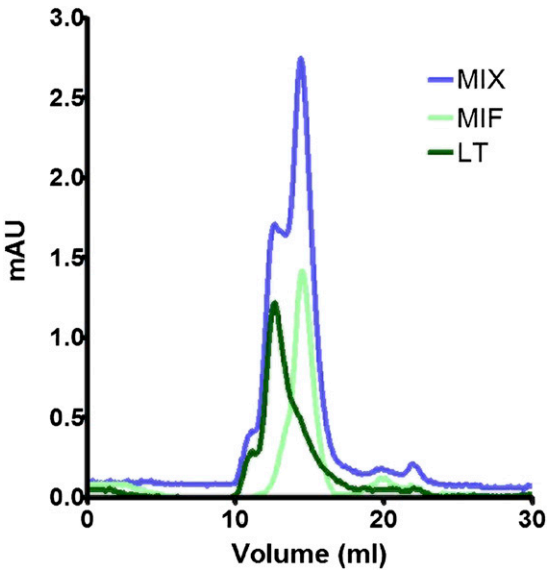

Fig. S2. SEC to examine potential interactions of a mixture of 200 μg WT MIF and 200 μg N110C. Each protein at the same concentration was loaded alone for comparison with the mixture. The S75 column (16/300) eluted peak for LT is at 12.63 mL and for MIF is at 14.43 mL alone and in the mixture.

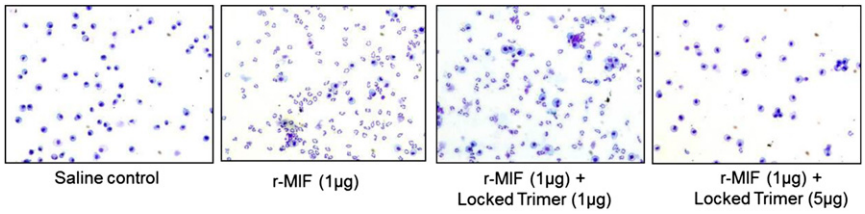

Fig. S3. Representative slides of the recovered cell population in BAL fluid stained with HEMA 3. r-MIF, recombinant murine MIF.

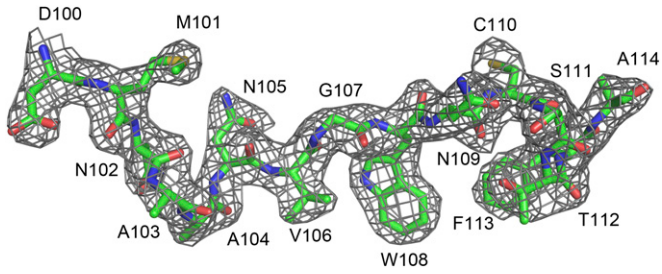

Fig. S4. Simulated annealing 2Fo–Fc electron density omit map at 3σ of the C-terminal tail of N110C. Oxygen, nitrogen, carbon, and sulfur atoms are red, blue, green, and gold, respectively.

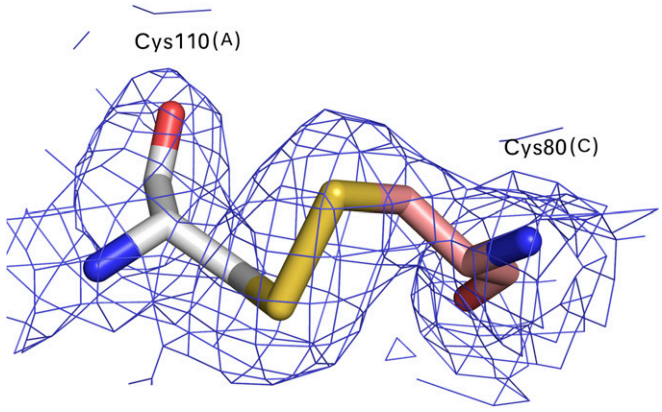

Fig. S5. Simulated annealing 2Fo–Fc electron density omit map at 3σ the disulfide between subunit A of trimer 1 Cys-80 and the mutant N110C of subunit C; this is typical electron density for the disulfide in all nine subunits in the unit cell. Oxygen, nitrogen, carbon, and sulfur atoms are red, blue, green, and gold, respectively.

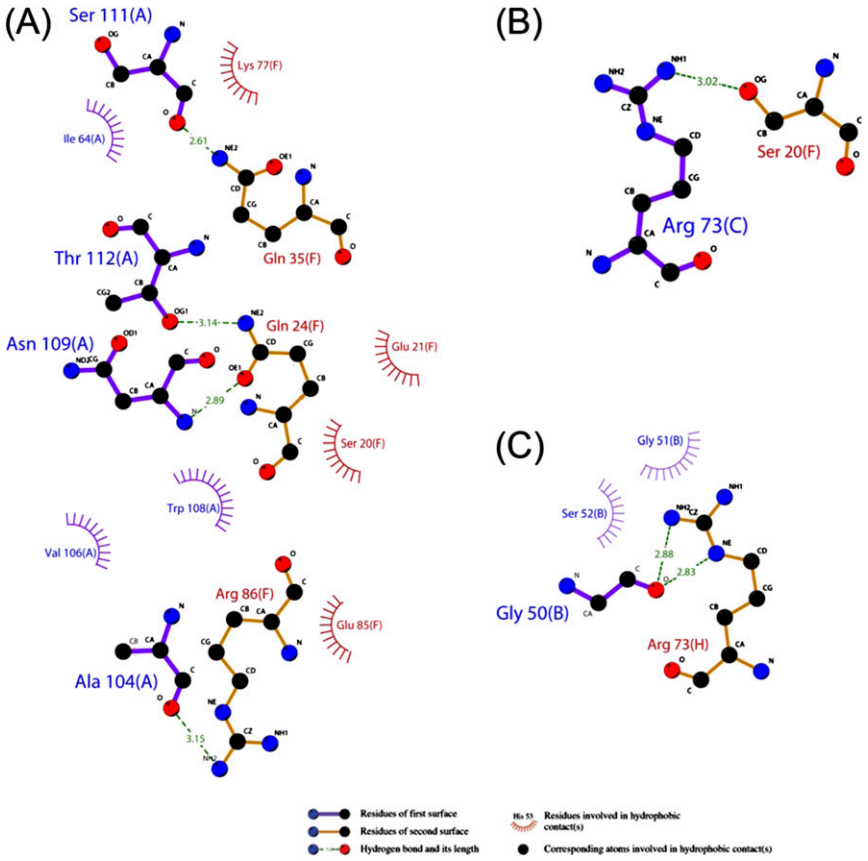

Fig. S6. Interactions between N110C trimer 1 with (*A* and *B*) trimer 2 and (*C*) trimer 3. Trimers 1, 2, and 3 are defined in Fig. 3*A*.

Table S1. Data collection and refinement statistics for the MIF C110N locked-trimer mutant

X-ray and refinement statistics	N110C-MIF (LT)*
Data collection	
Beamline	BNLS beamline X25
Wavelength (Å)	1.1
Space group	$P2_12_12_1$
Cell dimensions	
a, b, c, Å	50.31, 100.38, 199.48
Resolution (Å)	50–2.33 (2.41–2.33)
Rmsd	0.089 (0.597)
I/σ(I)	22.94 (4.95)
Completeness (%)	98.7 (99.1)
Redundancy	10.9 (11.2)
Refinement	
No. of observed reflections	473,150 (47,892)
No. of unique reflections	43,492 (4,276)
R_{work}/R_{free}	0.222 (0.272)
No. of atoms	
Protein atoms	7,399
Water	141
Ligand (chloride atom)	8
Total	7,548
B factors, Å^2	
Protein atoms	64.3
Water	57.7
Ligand/ion atoms	69.6
Rmsd from ideal bond parameters	
Bond lengths, Å	0.0028
Bond angles, °	0.648
Ramachandran, favored, generously allowed, disallowed, %	97.59, 2.21, 0.2

*Values in parentheses are for highest-resolution shell.

Table S2. Comparison of N110C monomer A with other subunits in the asymmetric unit and with WT MIF

Subunits	Length of alignment	Rmsd, Cα, Å	Length of alignment	Rmsd, Cα, Å
A and B	1–114	0.98	1–99	0.97
A–C	1–114	0.69	1–99	0.37
A–D	1–65, 68–114	0.48	1–65, 68–99	0.30
A–E	1–114	1.10	1–99	1.09
A–F	1–65, 68–105, 109–113	1.23	1–65, 68–99	0.40
A–G	1–32, 35–65, 68–114	1.50	1–32, 35–65, 68–99	1.20
A–H	1–64, 67–101, 110–111	1.26	1–64, 67–99	0.83
A–I	1–113	1.18	1–99	0.60
A–WT	1–114	3.33	1–99	1.17

These comparisons involve subunit A with other subunits (the total protein traced in electron density, column 2) as well as residues that lack the flexible C-terminal region (column 4).

Table S3. Comparison of N110C trimers in the asymmetric unit with each other and with WT MIF

Molecule A	Molecule B	Rmsd, Cα, Å
N110C trimer 1	N110C trimer 2	0.91
N110C trimer 1	N110C trimer 3	1.50
N110C trimer 2	N110C trimer 3	1.40
N110C trimer 1 (1–114)	WT (1–114)	3.56
N110C trimer 1 (1–99)	WT (1–99)	2.33